Superoscillatory $\mathcal{PT}$-symmetric potentials

Yaniv Eliezer,* Alon Bahabad, and Boris A. Malomed
Department of Physical Electronics, School of Electrical Engineering, Fleischman Faculty of Engineering, and Center of Light-Matter Interaction, Tel-Aviv University, Tel-Aviv 69978, Israel

(Received 5 August 2018; published 15 October 2018)

We introduce the one-dimensional $\mathcal{PT}$-symmetric Schrödinger equation, with complex potentials in the form of the canonical superoscillatory and suboscillatory functions known in quantum mechanics and optics. While the suboscillatorylike potential always generates an entirely real eigenvalue spectrum, its counterpart based on the superoscillatory wave function gives rise to an intricate pattern of $\mathcal{PT}$-symmetry-breaking transitions, controlled by the parameters of the superoscillatory function. One scenario of the transitions proceeds smoothly via a set of threshold values, while another one exhibits a sudden jump to the broken $\mathcal{PT}$ symmetry. Another noteworthy finding is the possibility of restoration of the $\mathcal{PT}$ symmetry, following its original loss, in the course of the variation of the parameters.

DOI: 10.1103/PhysRevA.98.043830

I. INTRODUCTION

The concept of complex-valued quantum Hamiltonians has been known for decades [1–4], yet for a long time it was commonly believed that a mandatory requirement for the reality of eigenvalues in a quantum system was the Hermiticity of the Hamiltonian. This belief was held firm in spite of producing several examples showing that complex Hamiltonians may generate a set of real eigenvalues [5–8] . It was the seminal work of Bender and Boettcher in 1998 [9] which showed that, by replacing the Hermiticity with the weaker condition of the $\mathcal{PT}$ symmetry, it is possible to construct classes of non-Hermitian Hamiltonians that exhibit completely real spectra of eigenvalues. An important principle found in this context is the necessary, yet not sufficient, condition for the $\mathcal{PT}$ symmetry, which states that a complex potential, if it is a part of the Hamiltonian, must satisfy the constraint $V(\xi) = V^*(-\xi)$, where ξ is the position coordinate. Many works examined different families of complex potentials satisfying this condition [9–16].

In the field of optics, the paraxial propagation of light in materials which include optical gain and loss can be modeled by the Schrödinger equation including a complex potential. As a consequence, it is possible to emulate the evolution of quantum $\mathcal{PT}$-symmetric systems in terms of classical optics. This concept was elaborated in numerous works [17–33] and demonstrated experimentally in various settings, such as optical waveguides [34–36], lasing [37], microcavity resonators [38], metamaterials [39], microwaves [40], electronic circuits [41], and acoustics [42].

Usually, $\mathcal{PT}$-symmetric potentials contain a control parameter, the variation of which leads to breaking of $\mathcal{PT}$ symmetry, at a certain threshold value of the parameter. Above the threshold, eigenstates of the $\mathcal{PT}$-symmetric Hamiltonian no longer remain eigenfunctions of the $\mathcal{PT}$ operator, and, at least, a subset of the spectrum of eigenvalues ceases to be real [9,43]. $\mathcal{PT}$-symmetry breaking was theoretically considered in various contexts and experimentally realized in optics [34,44–46].

Superoscillations are a phenomenon in which a band-limited signal oscillates locally faster than its highest Fourier component [47]. A canonical superoscillatory function was found by Aharonov *et al.* [48] in the theoretical framework of weak quantum measurements. A complementary canonical form for *suboscillatory* functions, i.e., signals which exhibit local oscillations that are slower than their lowest Fourier component, was recently found as well [49]. Superoscillations have found applications in various fields of optics, such as imaging [50–52], ultrafast optics [53,54], nonlinear light propagation [55], light-beam shaping [56–58], and optical traps [59].

In this work we first derive a potential for which the canonical superoscillatory function is an eigenstate of the Hamiltonian of the Schrödinger equation. The potential turns out to be a canonical suboscillatory function, and it is endlessly $\mathcal{PT}$ symmetric, always generating an entirely real spectrum of eigenvalues. Then we consider the superoscillatory complex canonical function itself as a complex $\mathcal{PT}$-symmetric potential. Varying its parameters, we report an intricate picture of $\mathcal{PT}$-symmetry-breaking phase transitions. In particular, there are regions in the parameter space where the variation leads to gradual expansion of the complex ($\mathcal{PT}$-symmetry-broken) part of the spectrum, while in other regions one can find paths for changing the parameters that lead to abrupt $\mathcal{PT}$-symmetry breaking. Furthermore, there are regions in which the initial symmetry breaking is followed by its restoration. The effects of broken $\mathcal{PT}$ symmetry on the evolution of localized field pulses are explored too by means of direct simulations.

II. ANALYSIS

A. Complex potential supporting the superoscillating wave function

First we consider the canonical superoscillatory function, devised originally in the context of weak measurements in

*yaniveli@post.tau.ac.il

 ©2018 American Physical Society

quantum mechanics [48,60]:

$$f_{\mathrm{SO}}(\xi) = [\cos(\xi) + ia\,\sin(\xi)]^N \equiv [g(\xi)]^N, \tag{1}$$

where a is a real parameter and N is an integer. We aim to identify it as a stationary wave function,

$$\psi(\xi,\eta) = e^{iE\eta}[\cos(\xi) + ia\,\sin(\xi)]^N, \tag{2}$$

of the scaled Schrödinger equation with a complex potential, $V(\xi)$:

$$i\psi_\eta = \psi_{\xi\xi} + V(\xi)\psi. \tag{3}$$

In terms of optics realization, η and ξ are, respectively, the longitudinal propagation distance and transverse spatial coordinate, while E is the propagation constant [61] ($-E$ would be the energy eigenvalue in the quantum model).

By substituting expression (2) into Eq. (3), we conclude that the wave function (2) is supported as an eigenstate, with the eigenvalue $E = N^2$, by the following potential:

$$V_{\mathrm{SO}}(\xi) = \frac{(a^2-1)N(N-1)}{[\cos(\xi) + ia\,\sin(\xi)]^2}. \tag{4}$$

The complex potential $V_{\mathrm{SO}}(\xi)$ is a $\mathcal{PT}$-symmetric one, as it is subject to the condition $V_{\mathrm{SO}}(\xi) = V^*_{\mathrm{SO}}(-\xi)$, with $*$ standing for complex conjugation [43]. In addition, this potential, which supports the canonical superoscillatory function as the stationary state of Schrödinger equation (3), can be identified as the known canonical suboscillatory function [49].

Because $V_{\mathrm{SO}}(\xi)$ is a complex periodic function, it can be expanded into the Fourier series:

$$V_{\mathrm{SO}}(\xi) = (a^2-1)N(N-1)\sum_{m=-\infty}^{+\infty} C_m \exp(im\xi), \tag{5}$$

where the coefficients C_n can be readily calculated:

$$C_m = \frac{1}{2\pi}\int_{-\pi}^{+\pi} \frac{\exp(-im\xi)}{[\cos(\xi) + ia\,\sin(\xi)]^2} d\xi = \begin{cases} -2m(a+1)^{\frac{m}{2}-1}(a-1)^{-\left(\frac{m}{2}+1\right)}, & m \in \{\text{even} < 0\}, \\ 0, & \text{otherwise.} \end{cases} \tag{6}$$

As shown by Bender *et al.* [10], any complex potential having a polynomial form in $\exp(i\xi)$ results in an entirely real spectrum. According to Eq. (6), the Fourier transform of $V_{\mathrm{SO}}(\xi)$ is discrete and completely single sided, i.e., the potential (5) is a polynomial of this type; hence, for all a and N, the respective energy spectrum remains endlessly real, with no occurrence of $\mathcal{PT}$-symmetry breaking. An example of potential $V_{\mathrm{SO}}(\xi)$ with parameters $N = 4$ and $a = 2$ is shown in Fig. 1. Note that the calculated energy bands for this case are indeed entirely real, and they include eigenvalue $E = N^2 = 16$, corresponding to the above-mentioned eigenfunction in the form of the canonical superoscillatory function.

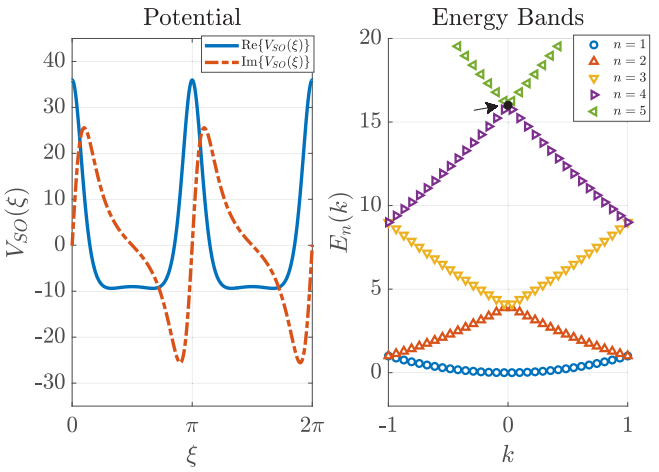

FIG. 1. Energy-band structure (right) of potential $\mathbf{V_{SO}}(\xi)$ (left), calculated for $\mathbf{N = 4}$, $\mathbf{a = 2}$. A black arrow marks the location where $E = N^2$.

B. Complex potential in the form of the canonical superoscillating function

We now consider the complex potential which itself has the form of the canonical superoscillatory function,

$$V_{\mathrm{SOF}}(\xi) = [\cos(2\xi) + ia\,\sin(2\xi)]^N, \tag{7}$$

where the above constraints on the parameters a and N are relaxed, both being taken as a pair of positive rational numbers. This form can be regarded as a generalization of previously examined real and $\mathcal{PT}$-symmetric potentials, viz., ones in the form of $\cos^N(\xi)$ (for $a = 0$ and positive integer N), $i\,\sin^N(\xi)$ (for $a \gg 1$ and odd integer N) [10,43], $4[\cos^2(\xi) + ia\,\sin(2\xi)]$ ($a > 1$, $N = 1$) [45], and $\exp(iN\xi)$ (for $a = 1$ and positive integer N) [10,62]. Since N may now be a fractional power, the complex potential (7) may be a multivalued function. To remove the complex-roots ambiguity, we select the following relation to uniquely define $V_{\mathrm{SOF}}(\xi)$:

$$\begin{aligned} V_{\mathrm{SOF}}(\xi) &= \exp\left(N\left[\ln|g(\xi)| + i\,\mathrm{atan}_2\left(\frac{\mathrm{Im}\{g(\xi)\}}{\mathrm{Re}\{g(\xi)\}}\right)\right]\right) \\ &= \exp\left(N\left\{\frac{1}{2}\ln[\cos^2(2\xi) + a^2\sin^2(2\xi)] \right.\right. \\ &\quad \left.\left. + i\,\mathrm{atan}_2[a\,\tan(2\xi)]\right\}\right), \end{aligned} \tag{8}$$

where $g(\xi)$ is the same as in Eq. (1), and $\mathrm{atan}_2(\cdot)$ is the "four-quadrant" inverse tangent, which is defined as the angle between the positive x axis and the vector ending at point $(\mathrm{Re}\{g(\xi)\}, \mathrm{Im}\{g(\xi)\})$. The resulting angle belongs to the interval $[0, \pi]$ for $\mathrm{Im}\{g(\xi)\} \geqslant 0$ and to $(-\pi, 0)$ for $\mathrm{Im}\{g(\xi)\} < 0$.

We use the numerically implemented Bloch-Floquet technique [63] to calculate the energy spectrum of potential (7) for various values of the parameters a and N. Unlike the complex potential of Eq. (4), the present one gives rise to $\mathcal{PT}$-symmetry breaking at sufficiently large values of a. To quantify this effect, we introduce a measure, $\rho_n(a, N)$, for the nth band of eigenvalues E, which quantifies a relative degree

of the $\mathcal{PT}$-symmetry breaking in the band, by calculating the portion of the Brillouin zone, $-1 < k < +1$ (of the corresponding quasimomentum k) in which the eigenvalues are complex:

$$\rho_n(a, N) = \frac{1}{2}\int_{-1}^{+1} I_n(k, a, N)dk, \tag{9}$$

with $\mathrm{I_n}(k, a, N)$ defined as

$$I_n(k, a, N) = \begin{cases} 1, & \mathrm{Im}[E_n(k, a, N)] > \varepsilon, \\ 0, & \mathrm{Im}[E_n(k, a, N)] \leqslant \varepsilon, \end{cases} \tag{10}$$

where ε is an arbitrarily chosen small number (we fix $\varepsilon = 10^{-6}$).

The measure was calculated in the first energy band for a set of parameter values in the range of $0 < a \leqslant 4$, $0 < N \leqslant 8$. This procedure produces a map indicating the relative degree of $\mathcal{PT}$-symmetry breaking within the examined range, which is displayed in Fig. 2. It shows that the spectrum remains real for even integer values of N in Eq. (7), while it is obvious that symmetry breaking takes place when N is an odd integer. Generally, as the parameter a increases (starting at zero), a threshold is crossed at some point at which symmetry breaking sets in, while the further growth of this parameter increases the symmetry-breaking degree, until eventually all the real eigenvalues in the first band are eliminated.

Here, we focus on the analysis for the first (lowest) energy band, as $\mathcal{PT}$ symmetry is, generally, more fragile in higher ones, making the situation less physically relevant. Nevertheless, some results for the second band are displayed in Fig. 3.

The particular case of potential (7) with $a = 1$ and integer N, i.e., $V_{\mathrm{SOF}}(\xi) = \exp(iN\xi)$, was studied previously [62]. Further, for $N = 1$ the latter potential is tantamount to the well-known one, $V = 4[\cos^2(\xi) + ia\,\sin(2\xi)]$, which has been examined in detail [45,46] (the dc [constant] component in V may be eliminated by an overall energy shift). The map displayed in Fig. 2 demonstrates that, in some intervals of values of N, such as $0 < N < 2$, the increase in a leads to crossing of the $\mathcal{PT}$-symmetry-breaking threshold, while the breaking measure, ρ_1, keeps growing with the further increase of a. However, at other values of N the dependence on a may be nonmonotonous. For instance, at $N = 2.5$ the further increase of a beyond the symmetry-breaking threshold brings the system back to the unbroken $\mathcal{PT}$-symmetry phase, with an entirely real energy spectrum. In this case, the subsequent increase of a up to, at least, $a = 8$ (the largest value for which the computation was performed) does not lead to a new symmetry-breaking event. In this connection, it is relevant to mention that examples of the restoration of the once broken $\mathcal{PT}$ symmetry with the continuing increase of a relevant control parameter (typically, it is the strength of the gain-loss terms) are known in some completely different systems, such as nonlinear $\mathcal{PT}$-symmetric models [64], nano-optical (subwavelength) $\mathcal{PT}$-symmetric media [65], and in scattering and lasing models as well [32,33]. Further, recall that even integer values of N are exceptional, as the symmetry breaking does not take place for them.

Our next observation is a very sharp transition between the $\mathcal{PT}$-symmetric and broken-symmetry phases at $a > 2.2$

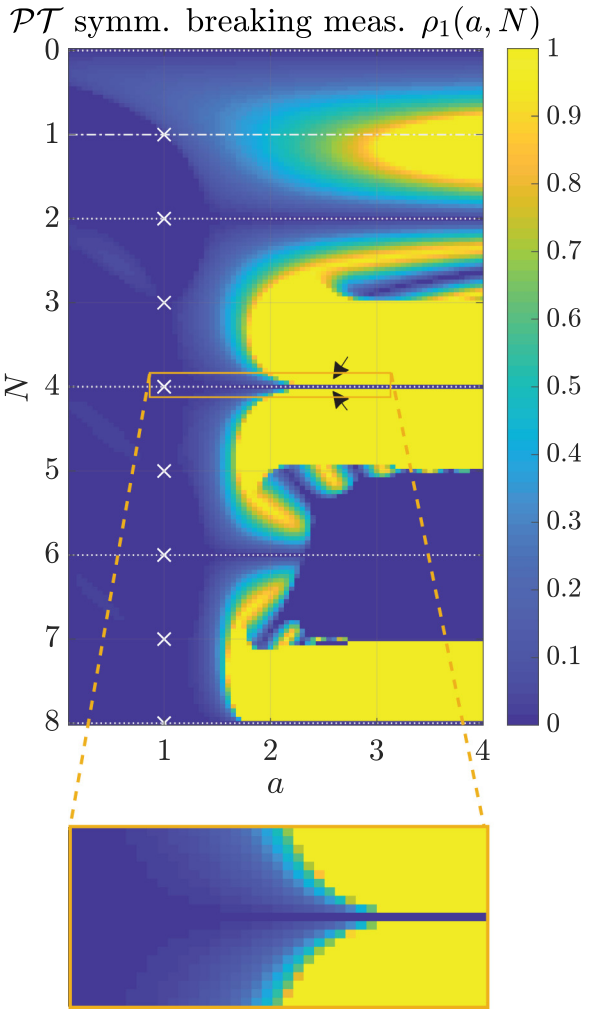

FIG. 2. $\mathcal{PT}$-symmetry breaking measure $\rho_1(\mathbf{a}, \mathbf{N})$. The darkest (brightest) color, corresponding to $\rho_1(a, N) = 0$ [$\rho_1(a, N) = 1$], shows the domain of parameters where the first band is entirely real (complex). Some specific cases of interest are marked, including positive integer N at $a = 1$, where potential (7) is $\exp(iN\xi)$ (white crosses), even integer N (white dotted lines), $N = 1$ (the white dashed dotted line), and, finally, $N = 4$, $a = 2.5$ (black arrows), where a sharp $\mathcal{PT}$-symmetry transition is clearly observed in the lower subframe zooming this region.

in a vicinity of $N = 4$. For $N = 4$, the first energy band remains entirely real (as for all even N), while adding a small fractional part to N turns the real band into a completely complex-valued one, as can be seen in Fig. 3, which displays the calculated energy eigenvalues in the first and second bands for potential (7) with $a = 2.5$ and $N = 3.9$, 4.0, and 4.1. Note that the potentials seem almost identical in these three cases, while the difference in the energy-band structure is dramatic, including the $\mathcal{PT}$-symmetry breaking taking place at $N = 3.9$ and 4.1, but absent at $N = 4$. The smallness of $|N - 4|$ may be a reason for virtually constant values of the imaginary eigenvalues across the Brillouin zone, which may be a subject for additional analysis.

To further examine the sharp transition, we use a well-known technique [10,66] to perform Floquet analysis of solutions to the Schrödinger equation with potential (7).

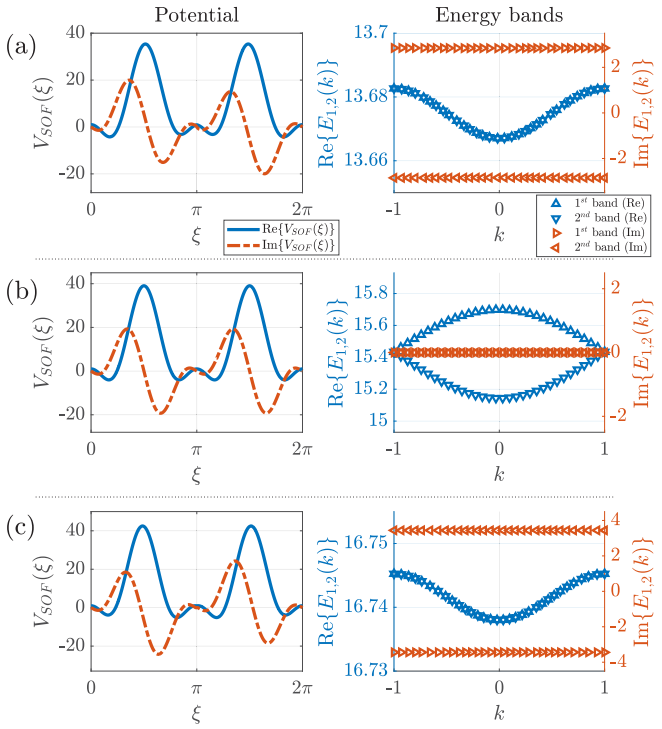

FIG. 3. Eigenvalue-band structure for selected potentials. Here, $a = 2.5$, while (a) $N = 3.9$, (b) $N = 4.0$, and (c) $N = 4.1$. Left column: the real (blue line) and imaginary (red dashed line) parts of each potential. Right column: the band diagrams showing the real and imaginary parts of the eigenvalues in the first and second bands.

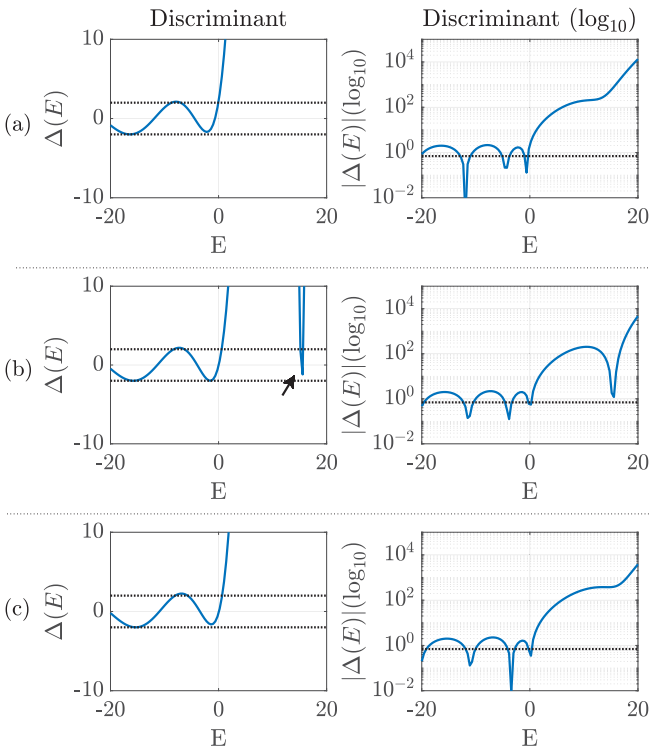

FIG. 4. Calculated discriminant function $\mathbf{\Delta}(\mathbf{E})$, which determines the existence of Bloch wave functions corresponding to real eigenvalues, for $a = 2.5$ and (a) $N = 3.9$, (b) $N = 4.0$, and (c) $N = 4.1$. Dotted vertical lines mark the boundaries $\Delta(E) = \pm 2$ indicating the existence area for the wave functions. The arrow marks a sharp minimum at $E \approx 15.56$.

Accordingly, stationary wave functions $\psi_k(\xi)$ are represented by a linear combination of two mutually orthogonal basis functions: $\psi_k(\xi) = c_k u_1(\xi) + d_k u_2(\xi)$, which are subject to the following boundary conditions:

$$u_1(0) = 1, \quad u_1'(0) = 0,$$
$$u_2(0) = 0, \quad u_2'(0) = 1, \tag{11}$$

We have found the basis functions as numerical solutions to the stationary Schrödinger equation, including potential (7) with $a = 2.5$ and $N = 3.9$, 4.0, or 4.1. According to the Floquet analysis, the solution $\psi_k(\xi)$, satisfying the Bloch condition, $\psi_k(\xi + \Lambda) = e^{ik\Lambda}\psi_k(\xi)$, with the potential's period Λ (in the present notation, $\Lambda = \pi$), is bounded provided that the discriminant, $\Delta(E) \equiv u_1(\Lambda) + u_2'(\Lambda)$, is real and meets the constraint $|\Delta(E)| \leqslant 2$. When this criterion is satisfied, there exists a real-valued band of eigenvalues. Figure 4 shows the calculated discriminant $\Delta(E)$ as a function of the energy for each one of the three cases, $N = 3.9$, 4.0, and 4.1. It is seen that, in the cases of $N = 3.9$ and $N = 4.1$ (the top and bottom rows) the discriminant's condition breaks for $E > 0$, on the contrary to the case of $N = 4.0$, where a sharp minimum appears in the region of $6 < E < 7$, allowing for the boundedness of $\psi(\xi)$ and for the existence of a real-energy band. Further calculation of the real-energy bandwidth $[\max(E_n) - \min(E_n)]$ for $N = 4.0$ exhibits an exponential decrease as the a parameter increases. We attribute the narrowing of the band to the exponential decrease in the magnitude of the superoscillatory feature in the imaginary part of the potential and to the increase of the maxima magnitude in the real part.

Next, we used the Crank-Nicolson algorithm [67] to simulate the evolution of a wide Gaussian wave packet, set initially around $\eta = 0$, governed by Eq. (3), again with the potential (7) corresponding to $a = 2.5$ with $N = 3.9$, 4.0, and 4.1. Figure 5 displays the evolution of the local intensity of the wave packet, $|\psi(\xi, \eta)|^2$, in each case. The blowup (exponential

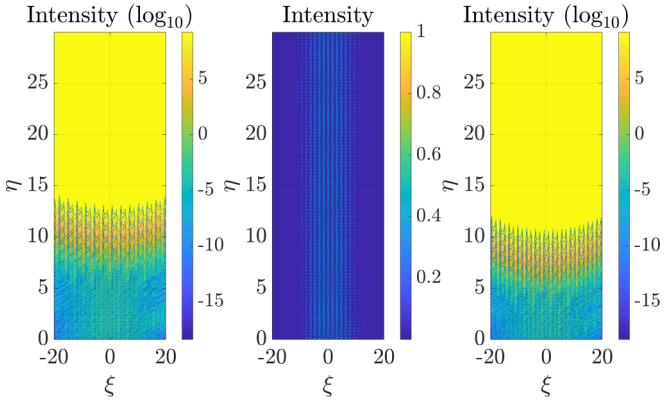

FIG. 5. Simulated evolution of the local intensity of the broad initial Gaussian, displayed for potential (7) with $a = 2.5$ and $N = 3.9$ (left), $N = 4.0$ (center), and $N = 4.1$ (right). In the left and right panels, the log scale is used.

growth of the field's amplitude) is, quite naturally, observed in the cases of broken $\mathcal{PT}$ symmetry, corresponding to $N = 3.9$ and 4.1 (the left and right panels in Fig. 5), while, in the absence of symmetry breaking ($N = 4.0$, the central panel), the wave packet retains a stable shape.

To complete the picture presented in Fig. 2, we finally consider the case of $a = 0$ and $0 \leqslant N \leqslant 8$, i.e., the potentials in the form of $V_{\mathrm{SOF}}(\xi) = \cos^N(2\xi)$. In the case when N is an integer, this potential is clearly Hermitian, generating real energy spectra, while when N is a rational fraction, the potential is multivalued and generally complex. Yet, unlike the case of $a \neq 0$, where the entire potential is complex valued, a fractional power of $\cos(2\xi)$ produces roots which are entirely real or piecewise real and complex. For any positive value of $\cos(2\xi)$, real roots always exist, while for $\cos(2\xi) < 0$ a real root exists if N is represented by an irreducible rational fraction, whose denominator is an odd integer:

$$N = P/Q, \quad Q = 1 + 2M \tag{12}$$

(M is an arbitrary integer). Thus one can construct the potential as a set of real roots, in case they are available, adding complex roots with the smallest phase when real roots are absent. Naturally, when Eq. (12) holds, the entire potential is real, producing a fully real eigenvalue spectrum. On the other hand, when Q in expression (12) is even, the potential includes complex segments, which results in $\mathcal{PT}$-symmetry breaking in the entire first band. The conclusion is that condition (12), the validity of which has a sparse structure with respect to the rationals and is discontinuous everywhere, determines $\rho_1(0, N)$ as follows:

$$\rho_1(0, N) = \begin{cases} 0, & N = P/(1 + 2M), \\ 1, & \text{otherwise}, \end{cases} \tag{13}$$

which implies that the $\mathcal{PT}$-symmetry breaking measure $\rho_1(0, N)$ itself is discontinuous and sparse.

III. CONCLUSIONS

We have examined the properties of the canonical suboscillatory and superoscillatory complex wave functions from quantum mechanics, which are given by Eqs. (4) and (7), respectively, as $\mathcal{PT}$-symmetric potentials in the one-dimensional Schrödinger equation. In the former case, we have found that such a complex potential always generates a purely real spectrum of energy eigenvalues, avoiding $\mathcal{PT}$-symmetry breaking. A more interesting situation takes place in the latter case, where the complex potential (7) gives rise to intricate phenomenology of the $\mathcal{PT}$-symmetry breaking. Depending on values of the parameters, a and N in Eq. (7), we have found a wide region in which the symmetry breaking develops smoothly, with the increase of the control parameter a, and, on the other hand, a region exhibiting an extremely sharp transition from the phase of unbroken $\mathcal{PT}$ symmetry to broken symmetry. Another noteworthy finding is a possibility of the restoration of the originally broken $\mathcal{PT}$ symmetry with subsequent growth of the control parameter a. Direct simulations of the evolution of input field pulses demonstrate their stability in the case of the unbroken symmetry, and a blowup when the symmetry was broken. Generally, our analysis shows that two families of complex potentials offer an essential extension of previously examined $\mathcal{PT}$-symmetric ones and suggests that the potentials may find application to waveguiding, lasing, filtering, and optical sensing. The refractive-index and gain-loss profiles emulating these potentials can be created by means of available experimental techniques.

As an extension of the present work reported, it may be interesting to consider a model combining the $\mathcal{PT}$-symmetric potentials with nonlinearity of the optical medium. A challenging direction for the development of the present analysis may be its extension to two-dimensional geometry.

[1] H. Feshbach, C. Porter, and V. Weisskopf, Model for nuclear reactions with neutrons, Phys. Rev. **96**, 448 (1954).

[2] G. Lindblad, On the generators of quantum dynamical semigroups, Commun. Math. Phys. **48**, 119 (1976).

[3] E. C. G. Sudarshan, C. B. Chiu, and V. Gorini, Decaying states as complex energy eigenvectors in generalized quantum mechanics, Phys. Rev. D **18**, 2914 (1978).

[4] N. Moiseyev, P. Certain, and F. Weinhold, Resonance properties of complex-rotated Hamiltonians, Mol. Phys. **36**, 1613 (1978).

[5] E. Caliceti, S. Graffi, and M. Maioli, Perturbation theory of odd anharmonic oscillators, Commun. Math. Phys. **75**, 51 (1980).

[6] A. A. Andrianov, The large n expansion as a local perturbation theory, Ann. Phys. (NY) **140**, 82 (1982).

[7] T. Hollowood, Solitons in affine Toda field theories, Nucl. Phys. B **384**, 523 (1992).

[8] F. Scholtz, H. Geyer, and F. Hahne, Quasi-Hermitian operators in quantum mechanics and the variational principle, Ann. Phys. (N.Y.) **213**, 74 (1992).

[9] C. M. Bender and S. Boettcher, Real Spectra in Non-Hermitian Hamiltonians Having PT Symmetry, Phys. Rev. Lett. **80**, 5243 (1998).

[10] C. M. Bender, G. V. Dunne, and P. N. Meisinger, Complex periodic potentials with real band spectra, Phys. Lett. A **252**, 272 (1999).

[11] M. Znojil, PT-symmetric square well, Phys. Lett. A **285**, 7 (2001).

[12] C. M. Bender, D. C. Brody, and H. F. Jones, Complex Extension of Quantum Mechanics, Phys. Rev. Lett. **89**, 270401 (2002).

[13] A. Khare and U. Sukhatme, Analytically solvable PT-invariant periodic potentials, Phys. Lett. A **324**, 406 (2004).

[14] A. Khare and U. Sukhatme, Complex periodic potentials with a finite number of band gaps, J. Math. Phys. **47**, 062103 (2006).

[15] N. Moiseyev, *Non-Hermitian Quantum Mechanics* (Cambridge University Press, Cambridge, UK, 2011).

[16] C. M. Bender, Rigorous backbone of symmetric quantum mechanics, J. Phys. A **49**, 401002 (2016).

[17] M. Berry and D. O'Dell, Diffraction by volume gratings with imaginary potentials, J. Phys. A **31**, 2093 (1998).

[18] A. Ruschhaupt, F. Delgado, and J. Muga, Physical realization of-symmetric potential scattering in a planar slab waveguide, J. Phys. A **38**, L171 (2005).

[19] R. El-Ganainy, K. Makris, D. Christodoulides, and Z. H. Musslimani, Theory of coupled optical PT-symmetric structures, Opt. Lett. **32**, 2632 (2007).

[20] M. Berry, Optical lattices with PT symmetry are not transparent, J. Phys. A **41**, 244007 (2008).

[21] S. Klaiman, U. Günther, and N. Moiseyev, Visualization of Branch Points in PT-Symmetric Waveguides, Phys. Rev. Lett. **101**, 080402 (2008).

[22] S. Longhi, Bloch Oscillations in Complex Crystals with PT Symmetry, Phys. Rev. Lett. **103**, 123601 (2009).

[23] T. Kottos, Optical physics: Broken symmetry makes light work, Nat. Phys. **6**, 166 (2010).

[24] R. Driben and B. A. Malomed, Stability of solitons in parity-time-symmetric couplers, Opt. Lett. **36**, 4323 (2011).

[25] H. Ramezani, T. Kottos, V. Kovanis, and D. N. Christodoulides, Exceptional-point dynamics in photonic honeycomb lattices with PT symmetry, Phys. Rev. A **85**, 013818 (2012).

[26] S. V. Suchkov, S. V. Dmitriev, B. A. Malomed, and Y. S. Kivshar, Wave scattering on a domain wall in a chain of PT-symmetric couplers, Phys. Rev. A **85**, 033825 (2012).

[27] N. V. Alexeeva, I. V. Barashenkov, A. A. Sukhorukov, and Y. S. Kivshar, Optical solitons in PT-symmetric nonlinear couplers with gain and loss, Phys. Rev. A **85**, 063837 (2012).

[28] H. Ramezani, T. Kottos, R. El-Ganainy, and D. N. Christodoulides, Unidirectional nonlinear $\mathcal{PT}$-symmetric optical structures, Phys. Rev. A **82**, 043803 (2010).

[29] A. A. Sukhorukov, Z. Xu, and Y. S. Kivshar, Nonlinear suppression of time reversals in PT-symmetric optical couplers, Phys. Rev. A **82**, 043818 (2010).

[30] S. Longhi and G. Della Valle, Photonic realization of PT-symmetric quantum field theories, Phys. Rev. A **85**, 012112 (2012).

[31] S. Longhi and G. Della Valle, Optical lattices with exceptional points in the continuum, Phys. Rev. A **89**, 052132 (2014).

[32] Y. D. Chong, L. Ge, and A. D. Stone, PT-Symmetry Breaking and Laser-Absorber Modes in Optical Scattering Systems, Phys. Rev. Lett. **106**, 093902 (2011).

[33] L. Pilozzi and C. Conti, Topological cascade laser for frequency comb generation in PT-symmetric structures, Opt. Lett. **42**, 5174 (2017).

[34] A. Guo, G. J. Salamo, D. Duchesne, R. Morandotti, M. Volatier-Ravat, V. Aimez, G. A. Siviloglou, and D. N. Christodoulides, Observation of $\mathcal{PT}$-Symmetry Breaking in Complex Optical Potentials, Phys. Rev. Lett. **103**, 093902 (2009).

[35] C. E. Rüter, K. G. Makris, R. El-Ganainy, D. N. Christodoulides, M. Segev, and D. Kip, Observation of parity–time symmetry in optics, Nat. Phys. **6**, 192 (2010).

[36] A. Regensburger, C. Bersch, M.-A. Miri, G. Onishchukov, D. N. Christodoulides, and U. Peschel, Parity–time synthetic photonic lattices, Nature (London) **488**, 167 (2012).

[37] H. Hodaei, M.-A. Miri, M. Heinrich, D. N. Christodoulides, and M. Khajavikhan, Parity-time–symmetric microring lasers, Science **346**, 975 (2014).

[38] B. Peng, Ş. K. Özdemir, F. Lei, F. Monifi, M. Gianfreda, G. L. Long, S. Fan, F. Nori, C. M. Bender, and L. Yang, Parity–time-symmetric whispering-gallery microcavities, Nat. Phys. **10**, 394 (2014).

[39] L. Feng, Y.-L. Xu, W. S. Fegadolli, M.-H. Lu, J. E. Oliveira, V. R. Almeida, Y.-F. Chen, and A. Scherer, Experimental demonstration of a unidirectional reflectionless parity-time metamaterial at optical frequencies, Nat. Mater. **12**, 108 (2013).

[40] Y. Liu, T. Hao, W. Li, J. Capmany, N. Zhu, and M. Li, Observation of parity-time symmetry in microwave photonics, Light Sci. Appl. **7**, 38 (2018).

[41] J. Schindler, A. Li, M. C. Zheng, F. M. Ellis, and T. Kottos, Experimental study of active LRC circuits with PT symmetries, Phys. Rev. A **84**, 040101 (2011).

[42] R. Fleury, D. Sounas, and A. Alù, An invisible acoustic sensor based on parity-time symmetry, Nat. Commun. **6**, 5905 (2015).

[43] C. M. Bender, Making sense of non-Hermitian Hamiltonians, Rep. Prog. Phys. **70**, 947 (2007).

[44] K. G. Makris, R. El-Ganainy, D. N. Christodoulides, and Z. H. Musslimani, Beam Dynamics in PT Symmetric Optical Lattices, Phys. Rev. Lett. **100**, 103904 (2008).

[45] K. G. Makris, R. El-Ganainy, D. N. Christodoulides, and Z. H. Musslimani, $\mathcal{PT}$ symmetric optical lattices, Phys. Rev. A **81**, 063807 (2010).

[46] K. Makris, R. El-Ganainy, D. Christodoulides, and Z. H. Musslimani, $\mathcal{PT}$-symmetric periodic optical potentials, Int. J. Theor. Phys. **50**, 1019 (2011).

[47] M. Berry, Faster than Fourier, Quantum Coherence and Reality: In Celebration of the 60th Birthday of Yakir Aharonov, *Proceedings of the International Conference on Fundamental Aspects of Quantum Theory* (World Scientific Publishing, Singapore, 1994), p. 55.

[48] Y. Aharonov, D. Z. Albert, and L. Vaidman, How the Result of a Measurement of a Component of the Spin of a Spin-1/2 Particle Can Turn Out to be 100, Phys. Rev. Lett. **60**, 1351 (1988).

[49] Y. Eliezer and A. Bahabad, Super defocusing of light by optical sub-oscillations, Optica **4**, 440 (2017).

[50] F. M. Huang, Y. Chen, F. J. G. de Abajo, and N. I. Zheludev, Optical super-resolution through super-oscillations, J. Opt. A: Pure Appl. Opt. **9**, S285 (2007).

[51] E. T. Rogers, J. Lindberg, T. Roy, S. Savo, J. E. Chad, M. R. Dennis, and N. I. Zheludev, A super-oscillatory lens optical microscope for subwavelength imaging, Nat. Mater. **11**, 432 (2012).

[52] A. M. Wong and G. V. Eleftheriades, An optical super-microscope for far-field, real-time imaging beyond the diffraction limit, Sci. Rep. **3**, 1715 (2013).

[53] Y. Eliezer, L. Hareli, L. Lobachinsky, S. Froim, and A. Bahabad, Breaking the Temporal Resolution Limit by Superoscillating Optical Beats, Phys. Rev. Lett. **119**, 043903 (2017).

[54] Y. Eliezer, B. K. Singh, L. Hareli, A. Arie *et al.*, Experimental realization of structured super-oscillatory pulses, Opt. Express **26**, 4933 (2018).

[55] R. Remez and A. Arie, Super-narrow frequency conversion, Optica **2**, 472 (2015).

[56] E. Greenfield, R. Schley, I. Hurwitz, J. Nemirovsky, K. G. Makris, and M. Segev, Experimental generation of arbitrarily shaped diffractionless superoscillatory optical beams, Opt. Express **21**, 13425 (2013).

[57] Y. Eliezer and A. Bahabad, Super-oscillating airy pattern, ACS Photon. **3**, 1053 (2016).

[58] T. Zacharias, B. Hadad, A. Bahabad, and Y. Eliezer, Axial sub-Fourier focusing of an optical beam, Opt. Lett. **42**, 3205 (2017).

[59] B. K. Singh, H. Nagar, Y. Roichman, and A. Arie, Particle manipulation beyond the diffraction limit using structured super-oscillating light beams, Light Sci. Appl. **6**, e17050 (2017).

[60] M. Berry and S. Popescu, Evolution of quantum superoscillations and optical superresolution without evanescent waves, J. Phys. A **39**, 6965 (2006).

[61] A. Yariv, *Quantum Electronics*, 3rd ed. (John Wiley & Sons, New York, 1989).

[62] F. Cannata, G. Junker, and J. Trost, Schrödinger operators with complex potential but real spectrum, Phys. Lett. A **246**, 219 (1998).

[63] N. Ashcroft and N. Mermin, *Solid State Physics* (Saunders College Publishing, Philadelphia, 1976).

[64] Y. Lumer, Y. Plotnik, M. C. Rechtsman, and M. Segev, Nonlinearly Induced PT Transition in Photonic Systems, Phys. Rev. Lett. **111**, 263901 (2013).

[65] C. Huang, F. Ye, Y. V. Kartashov, B. A. Malomed, and X. Chen, PT symmetry in optics beyond the paraxial approximation, Opt. Lett. **39**, 5443 (2014).

[66] C. Chicone, *Ordinary Differential Equations with Applications* (Springer-Verlag, New York, 2006).

[67] J. Crank and P. Nicolson, A practical method for numerical evaluation of solutions of partial differential equations of the heat-conduction type, Adv. Comput. Math. **6**, 207 (1996).